*plating*, 4th ed., (Eds: M. Schlesinger, M. Paunovic), John Wiley & Sons, New York **2000**.
[2] Y. W. Su, C. H. Wu, C. C. Chen, C. D. Chen, *Adv. Mater.* **2003**, *15*, 49.
[3] M. P. Zach, K. H. Ng, R. M. Penner, *Science* **2000**, *290*, 2120.
[4] M. Wang, S. Zhong, X.-B. Yin, J.-M. Zho, R.-W. Peng, N.-B. Min, *Phys. Rev. Lett.* **2001**, *86*, 3827.
[5] a) Y. Xia, G. M. Whitesides, *Angew. Chem.* **1998**, *110*, 568. b) H. Sugimura, T. Hanji, K. Hayashi, O. Takai, *Adv. Mater.* **2002**, *14,* 524.
[6] *Electrochemical Technology: Innovation and New Developments* (Eds: N. Masuka, T. Osako, Y. Ito), Gordon and Breach, Amsterdam **1996**.
[7] T. A. Taton, G. L. Lu, C. A. Mirkin, *J. Am. Chem. Soc.* **2001**, *123*, 5164.
[8] J. A. Rogers, R. J. Jackmam, G. W. Whitesides, *Adv. Mater.* **1997**, *9*, 475.
[9] R. J. Jackmam, S. T Brittain, A. Adams, M. G. Prentiss, G. W. Whitesides, *Science* **1998**, *280*, 2089.
[10] S. Zhong, M. Wang, X.-B. Yin, J.-M. Zho, R.-W. Peng, N.-B. Min, *J. Phys. Soc. Jpn.* **2001**, *70*, 1452.
[11] a) C. A. Foss, M. J. Tierney, C. R. Martin, *J. Phys. Chem.* **1992**, *96*, 9001. b) S. A. Sapp, D. T. Mitchell, C. R. Martin, *Chem. Mater.* **1999**, *11*, 1183. c) C. R. Martin, *Science* **1994**, *266*, 1961.
[12] Y. C. Stephen, K. Chris, G. Jian, *Nature* **2002**, *417*, 853.
[13] K. Spratte, L. F. Chi, H. Riegler, *Europhys. Lett.* **1994**, *25*, 211.
[14] M. Gleiche, L. F. Chi, H. Fuchs, *Nature* **2000**, *403*, 173.
[15] M. Gleiche, L. F. Chi, E. Gedig, H. Fuchs, *ChemPhysChem* **2001**, *3*, 187.
[16] N. Lu, M. Gleiche, J. Zheng, S. Lenhert, B. Xu, L. F. Chi, H. Fuchs, *Adv. Mater.* **2002**, *14*, 1812.
[17] C. Leger, L. Servant, J. L. Bruneel, F. Argoul, *Physica A* **1999**, *263*, 305.
[18] V. Fleury, J. N. Chazalviel, M. Rosso, *Phys. Rev. Lett.* **1992**, *68*, 2492.
[19] F. Sagues, M. Q. Lopez-Salvans, J. Claret, *Phys. Rep.* **2000**, *337*, 97.
[20] M.-Z. Zhang, Y. Wang, S. Wang, G.-W. Yu, M. Wang, R.-W. Peng N.-B. Ming, *J. Phys.: Condens. Matter* **2004**, *16*, 695.
[21] V. V. Tsukruk, V. N. Bliznyuk, *Langmuir* **1998**, *14*, 446.
[22] P. Amirfeiz, S. Bengtsson, M. Bergh, E. Zanghellini, L. Börjessond, *J. Electrochem. Soc.* **2000**, *147*, 2693.
[23] I. V. Markov, *Crystal Growth for Beginners: Fundamentals of Nucleation, Crystal Growth and Epitaxy*, World Scientific, Singapore **1995**.

# Microcontact Printing of CdS/Dendrimer Nanocomposite Patterns on Silicon Wafers**

By *Xiao C. Wu*, *Alexander M. Bittner*,* and *Klaus Kern*

Most photonics and electronics applications will eventually require parallel structuring methods for the control of the spatial positioning of functional materials, for example, multicolor LEDs, color pixels for field-emission displays, or multichannel chemical sensors. μCP is an interesting alternative to standard patterning techniques (such as lithography) due to its speed, simplicity, cheapness, and capability for high spatial resolution.[1] Patterning of functional materials via μCP is mainly based on printing passivating self-assembled monolayers (SAMs)[2] rather than the functional materials themselves. The advantage is that the interaction mechanisms between substrate, stamp, and ink (solution or suspension to cover the stamp) are well studied.[3] However, progress has recently been made in direct printing of various functional materials.[4,5] In order to achieve this a compatible stamp–material–surface system is needed. Successful printing often requires detailed studies of various printing conditions such as ink species (functional material), concentration, printing time, and surface properties of both stamp and substrate.

Nanoparticles might play an important role in future technologies such as photovoltaics, switches, phosphors, LEDs, electronic data-storage systems, and sensors.[6] Parallel schemes for positioning of these nanoparticles in fixed arrays are the basis of such potential photonic and electronic devices.[7] However, the direct patterning of these nanoparticles from solution with standard patterning techniques, such as laser ablation of the material and deposition through a shadow mask, are cumbersome, since the nanoparticles are often protected by organic surfactants (stabilizers) that tend to desorb at elevated temperature. Because the surfactants are usually necessary to stabilize the particles and to improve their functionality, any patterning approach must be carried out at low temperatures and in a mild environment.

Dendrimers are highly branched, spherically shaped molecules[8] (when the number of generations (G) is greater than four—here we employ generation-eight dendrimers). They are composed of core, repetitive unit, and terminal groups. The repetitive unit, here $-N-(CH_2CH_2-CONHCH_2CH_2-)_2$, and the terminal group, here amine, can exhibit different functionalities according to requirements. Dendrimers can be used as nanoreactors for the synthesis of various nanoparticles, such as metals, semiconductors, and magnetic oxides.[9–12] Based on dendrimer architecture, terminal groups, the loading factor of metal ions in dendrimers, and ion–ion interactions, nanoparticles can grow inside a dendrimer (internal type),[9] outside a dendrimer (external type), or in both modes.[10]

The big advantage of printing such composites is that—through the terminal groups—dendrimers can form layers on various surfaces via electrostatic forces, hydrogen bonds, van der Waals interactions, or metal–ligand interactions.[13,14] We believe that organic dendrimers will become a promising host material for the synthesis of nanoparticles and for their subsequent controlled placement on surfaces. Here, we combine the functionality of dendrimers as nanoreactors with their facile adsorption on surfaces. We demonstrate direct printing of luminescent CdS/dendrimer nanocomposites on hydroxyl-terminated silicon wafers.

We found that dendrimers can easily be transferred from hydrophilic stamps to the hydroxyl-terminated substrate.[5] Figure 1a shows polyamidoamine (PAMAM) dendrimer (gen-

[*] Dr. A. M. Bittner, Dr. X. C. Wu, Prof. K. Kern
Max-Planck-Institut für Festkörperforschung,
Heisenbergstr. 1, D-70569 Stuttgart (Germany)
E-mail: a.bittner@fkf.mpg.de

[**] We thank Dr. Christina Wege, Department of Biology, Stuttgart University for help with recording luminescence patterns.


DOI: 10.1002/adma.200306040

ADVANCED MATERIALS

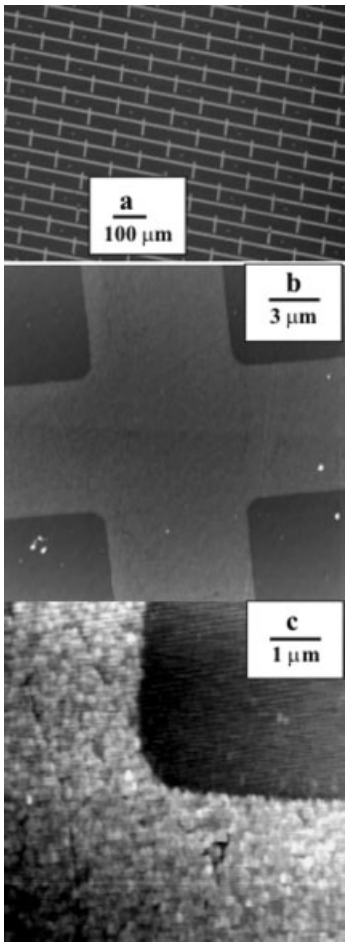


**Figure 1.** Electron micrograph (a), and topographic AFM images (b,c) of printed G8 $NH_2$ patterns on an oxidized silicon wafer. Ink: 2.5 μM G8 $NH_2$ dendrimer in ethanol.

eration 8) terminated with amine (denoted G8 $NH_2$) printed on a large area (the bright parts are G8 $NH_2$ molecules). It can be seen that G8 $NH_2$ molecules were successfully transferred to the substrate, exactly in the designed pattern. Fine details were revealed by atomic force microscopy (AFM). Figures 1b,c show topographic AFM images of a part of the pattern, obtained in the intermittent contact mode (IC-AFM). The cross-like protrusion (light gray parts) contains the printed dendrimers. From Figure 1c, we can see that G8 $NH_2$ molecules form a rather dense layer with dendrimers homogeneously distributed in the printed region. The height of the layer is 3–4 nm, similar to the thickness of a G8 $NH_2$ monolayer on hydrophilic surfaces.[14] The mean roughness of the printed layer is only about 0.5 nm at 5 μm scan size.

The ink concentrations were varied from 0.5–50 μM. It was found that a good pattern quality could be achieved with concentrations of 1–5 μM. Below 1 μM, an incomplete dendrimer coverage was observed. Above 5 μM of G8 $NH_2$, inhomogeneous multilayers with aggregates of dendrimers were obtained. The successful pattern transfer of G8 $NH_2$ is based on the formation of hydrogen bonds between the amine groups of the dendrimer and the hydroxyl groups of the substrate. The dendrimer–dendrimer interaction (in the dendrimer multilayer on the stamp) is obviously weaker than that between dendrimer and wafer, hence dendrimers can be printed.

We used the amine-terminated dendrimers as stabilizers for the growth of CdS nanoparticles, a potential material for blue photoluminescent devices and lasers. CdS/G8 $NH_2$ nanoparticle/dendrimer composites were synthesized by binding $Cd^{2+}$ ions only to the terminal amine groups. The CdS nanocomposite particles exhibit substantial aging at room temperature (RT), presumably due to Ostwald ripening, indicated by the rapid red shift of the absorption spectra (Fig. 2a) and the absorption bandgap (Figs. 2b,c). Note that pure G8 $NH_2$ and also internal type CdS/G8 OH[15] show no aggregation behavior, hence we infer an external-type composite here.

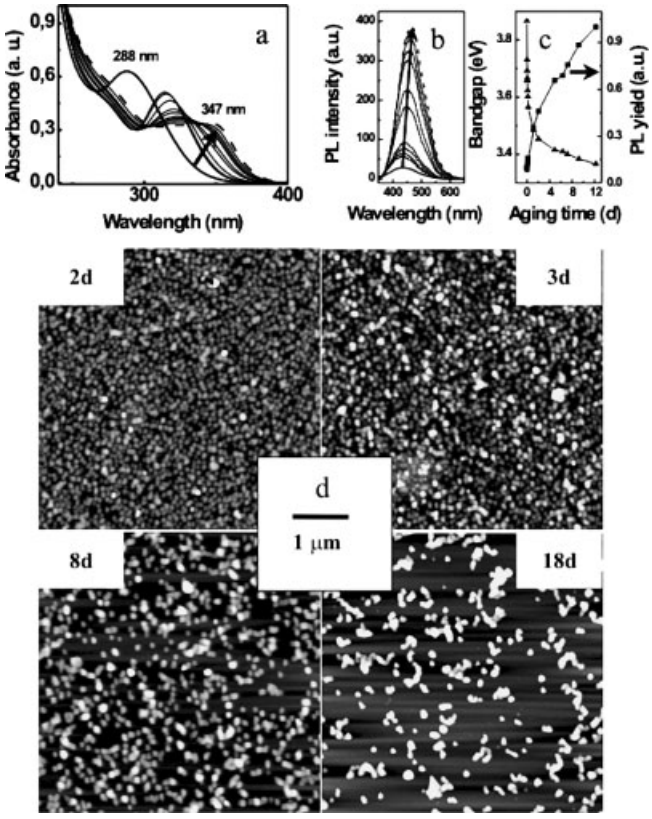


**Figure 2.** a) Evolution of absorption spectra of CdS/G8 $NH_2$ nanocomposites in methanol upon room temperature (RT) aging. Spectra were taken after 0, 100, 130, 255 min, 1, 2, 5, 6, 7, 9, and 12 days. b) Corresponding change in photoluminescence spectra (excited at 320 nm, optical path length 1 cm). c) Absorption bandgap (triangles) and photoluminescence yield (squares) versus RT aging time. d) Topographic AFM images of CdS/G8 $NH_2$ nanocomposites on oxidized silicon wafers. The composites were RT-aged 2, 3, 8, and 18 days in methanol before adsorption.

The photoluminescence (PL) from CdS nanoparticles is dominated by emission from a defect state, since the energy difference between the bandgap and the PL maximum is ~0.8 eV. With RT aging, the PL also shows a gradual red shift,

  

but the degree of the red shift is much less than that in the absorption spectra. This difference is due to the fact that larger CdS nanoparticles show more efficient photoluminescence (as seen in excitation spectra not shown here). Very small nanoparticles do not emit, possibly due to a large amount of nonradiative centers around their surface. The most obvious change in PL spectra is that the PL intensity increases with RT aging, as shown in Figures 2b,c. The PL yield can increase tenfold upon RT aging.

The Ostwald ripening growth also causes changes in the morphology of the nanocomposites. Figure 2d presents topographic IC-AFM images of nanocomposites that were aged before adsorption. During RT aging the particle heights increase from 10 nm to 60 nm, and the shape and size distributions broaden, suggesting the formation of supramolecular aggregates. The affinity to the oxidized silicon surface decreases. We term this stage "aged aggregates". The height of a single G8 $NH_2$ on a hydrophilic substrate is around 3 nm, while the diameter of the CdS nanoparticles was calculated to be ~2 nm (determined with the tight-binding approach or the pseudopotential method[16]). Fresh nanocomposites exist mainly as an aggregate of two or three G8 $NH_2$ molecules (judged from the height of AFM images) with several small CdS nanoparticles (judged from the calculated diameter of the nanoparticles by assuming one CdS per G8 $NH_2$). For aged aggregates, the morphology becomes more complicated due to aggregation processes. The AFM result we show here agrees with the results from other methods, such as TEM[11] and dynamic light scattering[11] for CdS/G4 dendrimer composites, and small angle X-ray and neutron scattering[12] for CuS/G4 dendrimer composites. Since pure G8 $NH_2$ molecules in methanol do not show this aggregation behavior, we believe that on the one hand the Ostwald ripening causes the growth of the CdS nanoparticles themselves, and on the other, it also causes the agglomeration of intact nanocomposites. This leads to the formation of supramolecular aggregates. Despite this aggregation, the CdS nanoparticles remain distinct entities (see UV/visible absorption spectra of Fig. 2a) and do not coalesce, because they are stabilized by the dendrimers.

CdS/G8 $NH_2$ nanocomposites, similar to dendrimers, can in principle be used as inks and transferred to hydroxyl-terminated substrates. Figure 3a is an electron micrograph of printed CdS/G8 $NH_2$ nanocomposites on a large area. Figures 3b,c are topographic IC-AFM images of the pattern. Similar to G8 $NH_2$ itself, these CdS/G8 $NH_2$ nanocomposites are also good inks and are easily transferred to the substrate: different from pure G8 $NH_2$, the nanocomposites do not form a dense layer. They show, however, a homogeneous distribution. As shown in Figure 2c, RT aging of nanocomposites can lead to a ~tenfold increase in PL efficiency. We observed PL patterns of printed aged nanocomposites with a fluorescence microscope. Figure 4a is a luminescence image of a CdS/G8 $NH_2$ pattern (aged nanocomposites). Control patterns formed from pure G8 $NH_2$ showed no luminescence images. The PL of the nanocomposites shows typical irreversible quenching on a timescale of 10 s, indicating fast oxidation of the CdS nanoparticles by oxygen under UV irradiation. However, the homogeneity of the luminescence intensity in the patterns is poor because we used a high ink concentration. We recorded topographic IC-AFM images (Fig. 4b) of the same sample (not at the same position). They prove that the distribution of nanocomposites on printed regions is indeed inhomogeneous.

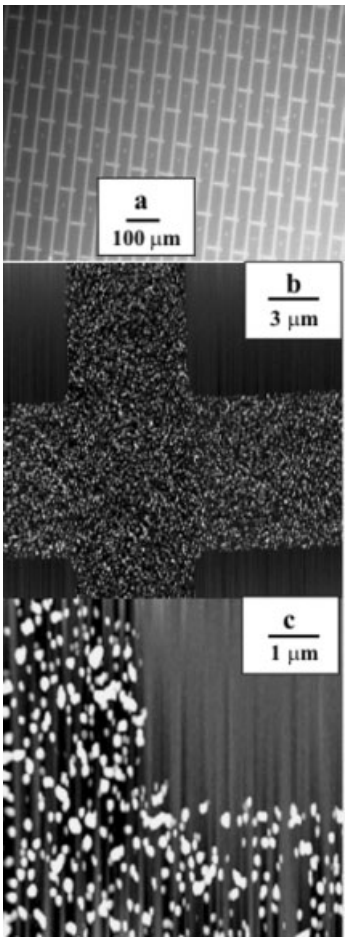


**Figure 3.** Electron micrograph (a), and topographic AFM images (b,c) of CdS/G8 $NH_2$ patterns on an oxidized silicon wafer, printed after 22 day RT aging in methanol. The feature size in the pattern is 8 μm. The ink concentration was 0.23 mM CdS (calculated from the added $S^{2-}$) in 1.83 μM G8 $NH_2$/methanol.

The successful printing of CdS/G8 $NH_2$ on a hydrophilic silicon wafer is based on the interactions between the amine groups of dendrimers and the hydroxyl groups on the silicon wafer. Since the CdS nanoparticles are located at the surface of the G8 $NH_2$ molecules, a certain fraction of the amine groups is directly bound to the nanoparticles. The unbound amine groups can form hydrogen bonds with hydroxyl groups on the surface. This leads to the successful transfer of nanoparticle composites from stamp to substrate. On the one hand the dendrimers act as stabilizers for CdS nanoparticles, on the other, they act as media between nanoparticles and the surface.

  

ADVANCED MATERIALS

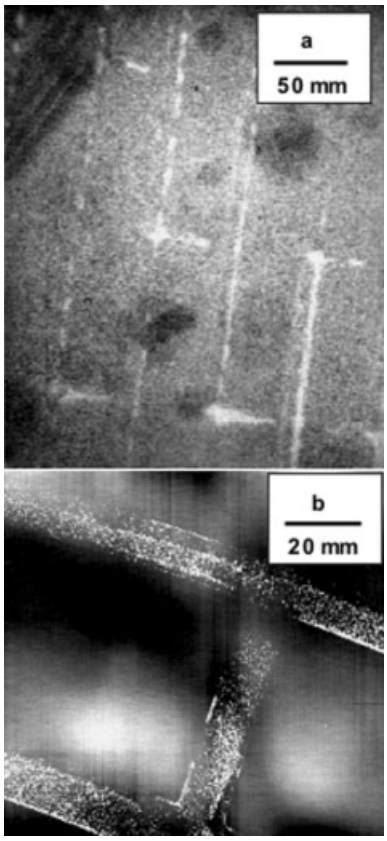


**Figure 4.** Fluorescence image (a), and topographic IC-AFM image (b) of printed aged CdS/G8 $NH_2$ nanocomposites on an oxidized silicon wafer.

Some further results indicate that indirect patterning of CdS/G8 $NH_2$ via solution adsorption is indeed as problematic as we had expected, e.g., we observed a much lower selectivity when the nanocomposites were adsorbed from solution on printed alkanethiolate patterns on gold: the bare gold and the thiolate patterns were both covered. In addition, the coverage on (unpatterned) solution-adsorbed thiolate was lower than on printed thiolate, presumably due to a lower ordering in the adsorbed thiolate layer.

## *Experimental*

Silicon wafers (orientation (100), Crystal, Berlin) were terminated by silicon oxide with hydroxyl groups by standard RCA procedure: 15 min immersion into a 340–350 K 1:1:5 mixture of 25 % $NH_4OH$ (VLSI Selectipur, Merck)/31 % $H_2O_2$ (VLSI Selectipur, Merck)/water (Millipore, 18 MΩcm); 15 min immersion into a 340–350 K 1:1:5 mixture of 37 % HCl (Suprapur, Merck)/30 % $H_2O_2$/water. We term these samples "oxidized silicon wafers". Poly(dimethylsiloxane) stamps (Sylgard 184, Dow Corning) were formed on flat polystyrene dishes or on patterned silicon wafer masters (IBM Zürich; before first use the master was rendered hydrophobic with fluoroalkyl-trichlorosilane vapor).

Polyamidoamine (PAMAM) dendrimer (generation 8) terminated with amine (Dendritech, Inc., Midland)), here referred to as G8 $NH_2$, was dissolved in 99.8 % ethanol (Roth) with concentrations 0.5 μM–50 μM. 200 μL G8 $NH_2$ was diluted with methanol to 10 mL (5.5 μM G8 $NH_2$), then 10 mL of 2 mM $Cd(CH_3COO)_2$ and 10 mL of 0.7 mM $Na_2S$ in methanol were added to the dendrimer solution sequentially. After reaction, the nanocomposites were stored in a –35 °C freezer to reduce the Ostwald ripening growth of nanoparticles. The final concentration of G8 $NH_2$ in the solution was 1.83 μM. The $Cd^{2+}/S^{2-}$ ratio was kept to 3:1 since it was found that at this ratio CdS/G8 $NH_2$ nanocomposites could be successfully printed. Before adsorption and printing, nanocomposites were dialyzed (Slide-A-Lyzer 10000 MWCO caps, KMF, Lohmar) against methanol.

A freshly activated flat stamp (150 mW (nominal), 1 mbar oxygen plasma for 10 s) was covered with one drop (20 μL) of ink solution for 25 s, and then blown dry with argon. A freshly activated structured stamp was brought into conformal contact with the inked flat stamp for 25 s, then peeled off and brought into conformal contact with a freshly cleaned silicon wafer for 25 s and peeled off from the substrate. All stamps were activated by oxygen plasma since pure dendrimers form large aggregates on hydrophobic surfaces. Control experiments for CdS/G8 $NH_2$ nanocomposites indicate that they form much larger aggregates on hydrophobic graphite surfaces than on hydrophilic silicon surfaces.

Absorption spectra were obtained with a Perkin Elmer UV/vis spectrometer Lambda 2. Photoluminescence and excitation spectra were taken with a Perkin Elmer luminescence spectrometer LS 50B. Atomic force microscope (AFM) images of patterns were obtained in intermittent contact mode with a Thermomicroscopes Autoprobe M5. Probes were ultrasharp noncontact silicon cantilevers from MikroMasch. Scanning electron microscope (SEM) images were taken with a JSM-6400 SEM operated at 20 kV. Fluorescence images were obtained on a Zeiss Axiophot miscroscope with a 400 nm excitation filter.

Received: August 19, 2003
Final version: November 17, 2003

[1] Y. Xia, G. M. Whitesides, *Angew. Chem. Int. Ed.* **1998**, *37*, 550.
[2] a) K. Ha, Y, Lee, D. Jung, J. Lee, K. Yoon, *Adv. Mater.* **2000**, *12*, 1614. b) Y. Koide, Q. Wang, J. Cui, D. P. Benson, T. J. Marks, *J. Am. Chem. Soc.* **2000**, *122*, 11 266. c) Y. Harada, X. Li, P. W. Bohn, R. G. Nuzzo, *J. Am. Chem. Soc.* **2001**, *123*, 8709.
[3] a) Y. Xia, G. M. Whitesides, *J. Am. Chem. Soc.* **1996**, *117*, 3274. b) E. Delamarche, H. Schmid, A. Bietsch, N. B. Larsen, H. Rothuizen, B. Michel, H. Biebuyck, *J. Phys. Chem. B* **1998**, *102*, 3324. c) T. Pompe, A. Fery, S. Herminghaus, A. Kriele, H. Lorenz, J. P. Kotthaus, *Langmuir* **1999**, *15*, 2398. d) K. R. Finnie, R. Haasch, R. G. Nuzzo, *Langmuir* **2000**, *16*, 6968.
[4] a) L. Yan, X. M. Zhao, G. M. Whitesides, *J. Am. Chem. Soc.* **1998**, *120*, 6179. b) J. Lahiri, E. Ostuni, G. M. Whitesides, *Langmuir* **1999**, *15*, 2055. c) H. Kind, J. M. Bonard, C. Emmenegger, L. O. Nilsson, K. Hernadi, E. Maillard-Schaller, L. Schlapbach, L. Forro, K. Kern, *Adv. Mater.* **1999**, *11*, 1285. d) A. Bernard, J. P. Renault, B. Michel, H. R. Bosshard, E. Delamarche, *Adv. Mater.* **2000**, *12*, 1067. e) Z. P. Yang, A. M. Belu, A. Vision, H. Sagg, A. Chilkoti, *Langmuir* **2000**, *16*, 7482. f) H. Kind, H. M. Geissler, H. Schmid, B. Michel, K. Kern, E. Delamarche, *Langmuir* **2000**, *19*, 6367. g) D. Arrington, M. Curry, S. C. Street, *Langmuir* **2002**, *18*, 7788.
[5] X. C. Wu, A. M. Bittner, K. Kern, *Langmuir* **2002**, *18*, 4984.
[6] A. P. Alivisatos, *Science* **1996**, *271*, 933.
[7] C. H. Lu, N. Z. Wu, F. Wei, X. S. Zhao, X. M. Jiao, J. Xu, C. Q. Luo, W. X. Cao, *Adv. Funct. Mater.* **2003**, *13*, 548.
[8] F. Zeng, S. C. Zimmerman, *Chem. Rev.* **1997**, *97*, 1681.
[9] a) L. Balogh, D. A. Tomalia, *J. Am. Chem. Soc.* **1998**, *120*, 7355. b) M. Q. Zhao, L. Sun, R. M. Crooks, *J. Am. Chem. Soc.* **1998**, *120*, 4877. c) M. Q. Zhao, R. M. Crooks, *Angew. Chem. Int. Ed.* **1999**, *38*, 364. d) M. Q. Zhao, R. M. Crooks, *Chem. Mater.* **1999**, *11*, 3379.
[10] a) J. Zheng, M. S. Stevenson, R. S. Hikida, P. V. van Patten, *J. Phys. Chem. B* **2002**, 06, 1252. b) E. Strable, J. M. Bulte, B. Moskowitz, K. Vivekanandan, M. Allen, T. Douglas, *Chem. Mater.* **2001**, 13, 2201.
[11] K. Sooklal, L. H. Hanus, H. J. Ploehn, C. J. Murphy, *Adv. Mater.* **1998**, *10*, 1083.
[12] N. C. B. Tan, L. Balogh, S. F. Trevino, D. A. Tomalia, J. S. Lin, *Polymer* **1999**, *40*, 2537.

  

[13] a) W. M. Lackowski, J. K. Campbell, G. Edwards, V. Chechik, R. M. Crooks, *Langmuir* **1999**, *15*, 7632. b) H. Zhang, P. C. M. Grim, D. Liu, T. Vosch, S. De Feyter, U. M. Wiesler, A. J. Berresheim, K. Muellen, C. V. Haesendock, N. Vandamme, F. C. De Schryver, *Langmuir* **2002**, *18*, 1801.
[14] V. V. Tsukruk, F. Rinderspacher, V. N. Bliznyuk, *Langmuir* **1997**, *13*, 2171.
[15] B. I. Lemon, R. M. Crooks, *J. Am. Chem. Soc.* **2000**, *122*, 12 886.
[16] S. V. Gaponenko, *Optical Properties of Semiconductor Nanocrystals*, Cambridge University Press **1998**, p. 53.

# Two- and Three-Dimensional Ordered Structures of Hollow Silver Spheres Prepared by Colloidal Crystal Templating**

By *Zhuo Chen*, *Peng Zhan*, *Zhenlin Wang*,* *Jianhui Zhang*, *Weiyi Zhang*, *Naiben Ming*, *Che Ting Chan*, and *Ping Sheng*

Much attention has been focused recently on the preparation of macroporous materials by templating with colloidal crystals. This interest stems from the important properties of such microstructures, which have a wide range of applications including sensors, catalysts, and photonic crystals. Various macroporous and mesoporous materials have been made via this process, including ceramics,[1–9] carbon,[10,11] chalcogenides,[12–14] NaCl,[3] polymers,[15–19] and silica–gold.[20] The extension of such a material patterning method to metals is particularly attractive, as metals with ordered microstructures exhibit unique optical, electrical, magnetic, and catalytic properties. For example, surface enhancement of Raman scattering in porous gold films has been demonstrated by Tessire et al.[21] In a recent study, Baumberg and coworkers reported the observation of confined plasmons in gold nanocavities.[22]

Although the adaptation of the templating method to the preparation of porous metal films is limited, several strategies have been reported, including precipitation/chemical conversion,[23,24] direct penetration of metal nanocrystals,[25] electroless deposition,[26,27] and electrochemical reduction methods.[28] When monodispersed silica spheres are used as the sacrificial elements, annealing of the colloidal crystal is usually performed at high temperatures. This results in the formation of small necks between neighboring spheres, which makes the template stable during the material patterning process.[26–28] A complete filtration of metal into the free spaces of the template has been successfully demonstrated using these approaches, which result in macroporous metal films that are an exact replica of the sacrificial templates.

In this communication we report for the first time the preparation of ordered arrays of hollow metal spheres by colloidal crystal templating. However, instead of using annealed silica colloidal crystals as templates,[26–28] we use polymer colloidal crystals. Moreover, the template is confined between two substrates in order to preserve its ordering in the material-patterning process, as described by Xia and coworkers.[29] We combine a seeded growth technique for metal coatings on isolated colloids in solution and the confined template-directed synthesis method for material patterning. The samples we obtain are were two-dimensional (2D) and three-dimensional (3D) ordered hollow silver spheres prepared by templating against the monolayer or the multilayer of hexagonal close packed polymer beads, respectively.

The schematic procedure of our experiment is depicted in Figure 1. The starting material is an ordered colloidal crystal consisting of polystyrene (PS) beads, which was prepared using a modification of the micromolding method reported by Kim et al.[30] Specifically, a microchannel was first formed between two glass slides that were separated with two identical spacers. Upon dipping into a colloidal dispersion solution, the microchannel was spontaneously filled with the colloidal dispersion due to capillary forces. Nucleation occurred at the upper opening of the channel, which resulted in a self-organization of these microspheres. Evaporation of the solvent from the opening of the microchannel caused a continuous flow of the colloidal dispersion to the ordered area; as a consequence, a steady growth of colloidal crystal was achieved. It should be noted that in aqueous solution the ordered negatively charged PS beads are separated from each other due to the repulsive electrostatic forces between them.[29,31] When dried in air, cracks were often observed in the template due to a decrease in the hydrodynamic size of the particles. Previous studies[32,33] have shown that the magnitude of shrinkage is about 5–15 % of the particle size and is mainly determined by the strength of the repulsive force, which itself depends on the density of the charge on each particle and the concentration of free electrolyte in the solvent. Furthermore, in order to prevent the settlement of the spheres due to gravitational forces, especially for larger polymer beads, the colloidal dispersion should be stirred continuously during the colloidal crystal growth. The colloidal crystals obtained by this approach are a sequential stacking of planes consisting of hexagonal close packed spheres with the surface parallel to the substrate. The growth of high-quality films with an area of $5 \times 10$ mm takes about

[*] Prof. Z. L. Wang, Z. Chen, P. Zhan, Dr. J. H. Zhang, Prof. W. Y. Zhang, Prof. N. B. Ming
National Laboratory of Solid State Microstructures
Nanjing University
Nanjing 210093 (P.R. China)
E-mail: zlwang@nju.edu.cn
Prof. C. T. Chan, Prof. P. Sheng
Department of Physics
Hong Kong University of Science and Technology
Clear Water Bay, Hong Kong (P.R. China)

[**] The authors acknowledge the help of Dr. R. W. Peng and Dr. X. S. Wu for the characterization of these materials, and thank Dr. H. T. Wang for useful discussions. This work is supported by a grant for the State Key Program for Basic Research of China, NSFC under grant No. 10174031 and 90101030, and RGC through HKUST6145/99P. W. Z. acknowledges partial support from NSFC under the "Excellent Youth Foundation".

 DOI: 10.1002/adma.200306445  